Chemical Science

ROYAL SOCIETY OF CHEMISTRY

EDGE ARTICLE

View Article Online
View Journal | View Issue

Check for updates

Cite this: *Chem. Sci.*, 2023, **14**, 13944

All publication charges for this article have been paid for by the Royal Society of Chemistry

Received 22nd July 2023
Accepted 15th November 2023

DOI: 10.1039/d3sc03806h

rsc.li/chemical-science

Open Access Article. Published on 16 November 2023. Downloaded on 5/2/2026 7:54:51 PM.
This article is licensed under a Creative Commons Attribution 3.0 Unported Licence.

Group 13 ion coordination to pyridyl breaks the reduction potential *vs.* hydricity scaling relationship for dihydropyridinates†

Leo W. T. Parsons, James C. Fettinger and Louise A. Berben *

The relationship E_p *vs.* ΔG_{H-} correlates the applied potential (E_p) needed to drive organohydride formation with the strength of the hydride donor that is formed: in the absence of kinetic effects E_p *vs.* ΔG_{H-} should be linear but it would be more energy efficient if E_p could be shifted anodically using kinetic effects. Biological hydride transfers (HT) performed by cofactors including NADH and lactate racemase do occur at low potentials and functional modeling of those processes could lead to low energy HT reactions in electrosynthesis and to accurate models for cofactor chemistry. Herein we probe the influence of *N*-alkylation or *N*-metallation on ΔG_{H-} for dihydropyridinates (DHP^-) and on E_p of the DHP^- precursors. We synthesized a series of DHP^- complexes of the form ($pz_2{}^HP^-$)E *via* hydride transfer from their respective $[(pz_2P)E]^+$ forms where E = $AlCl_2{}^+$, $GaCl_2{}^+$ or Me^+. Relative ΔG_{H-} for the ($pz_2{}^HP^-$)E series all fall within 1 kcal mol^{-1}, and ΔG_{H-} for ($pz_2{}^HP$)CH_3 was approximated as 47.5 ± 2.5 kcal mol^{-1} in MeCN solution. Plots of E_p *vs.* ΔG_{H-} including $[(pz_2P)E]^+$ suggest kinetic effects shift E_p anodically by ~215 mV.

Introduction

Reduction reactions involving hydride transfer (HT, formally two electrons and a proton) are important in transformations ranging from CO_2 reduction[1,2] to selective reductions of carbonyls, imines, and alkenes.[3–5] In enzymes, tremendous selectivity and efficiency in reduction reactions involving HT is achieved by cofactors such as NAD^+/NADH and the nickel pincer nucleotide (NPN) cofactor in lactate racemase, in a carefully tailored environment.[6,7] Synthetic chemists have harnessed this control in systems which incorporate enzymes for highly efficient reactions in the presence of catalytic NAD^+,[8,9] and synthetic chemists aspire to similar reaction control as in the asymmetric co-catalysis of enantioselective organocatalytic hydride reduction.[10,11] Alongside these reaction conditions, a wide array of both metal hydride (M–H) and organohydride (C–H) transfer agents has been developed, and ongoing efforts have various directions: improved selectivity for desired products,[12–14] and functional group tolerance,[15,16] are just two examples.

In the growing area of electrosynthesis and electrocatalysis additional considerations need to be made for the design of HT reagents that can be effectively (re)generated electrochemically. These include choice of proton source for hydride regeneration and catalytic turnover and design of precursors to the hydride which lower the applied potential required for the reduction steps that (re)generate the hydride reagent in the catalytic cycle (Scheme 1).[17–19] The lowered potential is needed to save energy, and minimize side reactions including proton reduction to H_2 and decomposition of catalyst or substrate. It is well-known that the half wave potential, $E_{1/2}(D^{+/0})$ for the hydride precursor (D^+ in Scheme 1) scales with the free energy change associated with loss of hydride ion from a metal- or organo-hydride as in eqn (1):[20,21]

$$D{-}H \rightarrow D^+ + H^- \text{ free energy: } \Delta G_{H-} \quad (1)$$

This free energy change is also called hydricity (ΔG_{H-}). Experimentally, hydricity is determined using thermochemical

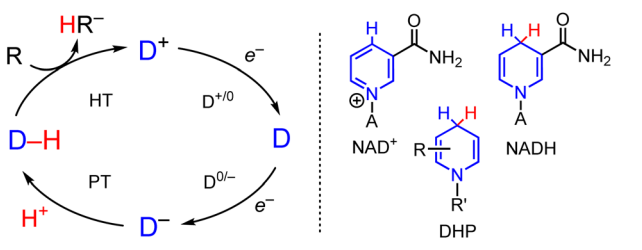

Scheme 1 (Left) Outline of electron and proton steps to generic cationic hydride precursor, D^+, leading to hydride formation of a general hydride donor D–H and subsequent HT to substrate. (Right) Line drawing of NAD^+, NADH and dihydropyridinate, DHP. A = Adenine dinucleotide.

Department of Chemistry, University of California, Davis, CA, 95616, USA. E-mail: laberben@ucdavis.edu

† Electronic supplementary information (ESI) available: Synthesis and characterization of compounds, ^1H and ^{13}C NMR, tables of crystallographic data, crystallographic data (CIF). CCDC 2278349 and 2278350. For ESI and crystallographic data in CIF or other electronic format see DOI: https://doi.org/10.1039/d3sc03806h

© 2023 The Author(s). Published by the Royal Society of Chemistry

Open Access Article. Published on 16 November 2023. Downloaded on 5/2/2026 7:54:51 PM.
This article is licensed under a Creative Commons Attribution 3.0 Unported Licence.

cycles that are well described in the literature,[22,23] and cycles relevant to this work are included below (*vide infra*).

Hydricity can be a useful predictor for the overall driving force for an HT reaction and influence reaction selectivity, where a smaller ΔG_{H-} value indicates a stronger thermodynamic driving force for HT, *i.e.* a stronger hydride donor. For example, electrocatalytic reduction of CO_2 to $HCOO^-$ is optimized when the hydride donor is sufficiently hydridic to make CO_2 reduction thermodynamically favorable but not so strong as to undergo competitive H_2 evolution *via* reaction of the hydride with protons.[24–27] Both $E_{1/2}$ and ΔG_{H-} are intrinsic thermodynamic properties of the hydride donor reagent.[28,29] In practice, reduction of D^+ is often coupled with proton transfer (PT) reactions and then the CV waveform manifests as an irreversible redox event where both thermodynamic and kinetic contributions to the $D^{+/0}$ and $D^{0/-}$ redox couples and PT influence the necessary applied potential (E_p) that is required to generate D–H.[30] Metal ion coordination is known qualitatively to lower E_p for organic molecules including DHP^-s but not enough data has been reported to draw any correlations between structure and function.[31,32]

In this report, we investigate structural tuning of dihydropyridinates (DHP^-) and their precursors *via* metal ion effects. To assess the results of metal ion coordination we considered the scaling relationship between E_p *vs.* ΔG_{H-} using extensive data reported in the literature, and as discussed below.[21,33,36] The dipyrazolylpyridine ligand platform (pz_2P) supports complexes with the form $[(pz_2P)E]^+$ where E = $GaCl_2^+$, CH_3^+ and $AlCl_2^+$, and those compounds are denoted herein as $\mathbf{1}^+$, $\mathbf{2}^+$ and $\mathbf{4}^+$ respectively.[30,36] In this report the syntheses of organohydrides ($pz_2{}^HP^-$)E, are reported for E = $GaCl_2^+$ and CH_3^+, *via* a formal addition of hydride (two electrons and one proton) to $[(pz_2P)E]^+$ (Scheme 2). Characterization of the geometric and electronic structures of **1H**, **2H** and **4H** was performed and the hydride donor ability for each compound benchmarked. A comparison of the properties of **1H** and **2H** with those of previously reported organohydride reagents reveals reduction potential is lowered by + 215 mV for **1H** and does not deviate within error for **2H** relative to E_p expected according to the E_p *vs.* ΔG_{H-} scaling relationship. The origin of this effect is discussed.

Results and discussion

Preparation of compounds

We targeted the 1,4-DHP^-'s derived from $[(pz_2P)GaCl_2]^+$ ($\mathbf{1}^+$) and $[(pz_2P)CH_3]^+$ ($\mathbf{2}^+$) (Scheme 3). In an attempt to generate $[(pz_2{}^HP^-)]GaCl_2$ (**1H**), two equivalents of Na were added to a solution of one equivalent pz_2P in THF at room temperature and the clear solution turned deep red following consumption of the Na metal over 24 h.[35] Addition of one equivalent of $GaCl_3$ resulted in a further colour change to dark purple. The ^{1}H NMR spectrum of the isolated product showed no resonances corresponding to protons on an aromatic pyridine ring but instead resonances at 5.21 and 3.57 ppm were observed. These resonances are consistent with a 1,4-DHP^- ligand form coordinated to $GaCl_2^+$, and consistent with our previous report of $[(pz_2{}^HP^-)]AlCl_2$, **4H**,[36] where the resonances were observed at 4.99 and 3.50 ppm. However, integration of the resonance at 3.57 ppm gives a value of **1**H atom for the C_p–H proton (see Fig. 1 for carbon atom labelling scheme), but integration of 2H atoms is expected for formation of **1H**. A multiplet at 1.76 and doublet at 1.12 ppm corresponding to integrations of 1H atom and 6H atoms, respectively, suggest substitution of an *i*Pr group at the C_p carbon (Fig. S1†), and this was confirmed by single crystal X-ray diffraction which identified $[(pz_2{}^{iPr}HP^-)]GaCl_2$ (**3H**), (*vide infra*). Presumably, a reductive cleavage of *N*-isopropyl generates isopropylsodium, which, in turn, reacts with the pyridine ring to form **3H**.[37]

Synthesis of 1H was also attempted *via* several additional routes

Reduction of $[(pz_2P)GaCl_2]GaCl_4$ (**1**-$GaCl_4$) was attempted *via* reactions with sodium metal, sodium napthalenide, and decamethylcobaltocene, but these reactions did not yield clean isolable products. Reactions of **1**-$GaCl_4$ with hydride donors $NaBH_4$, $LiAlH_4$, and $LiEt_3BH$ also did not yield **1H**. Ultimately, we obtained **1H** in 55% yield as crystals formed from a concentrated solution of **1**-$GaCl_4$ and **2H** in MeCN (the

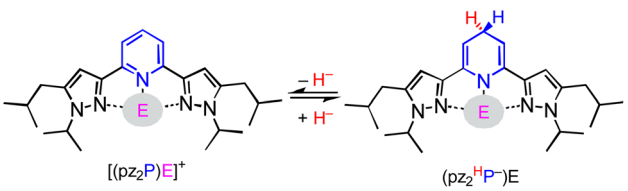

Scheme 2 Interconversion of $(pz_2P)E^+$ with $(pz_2HP^-)E$ *via* HT, where E = $AlCl_2^+$, $GaCl_2^+$, and CH_3^+.

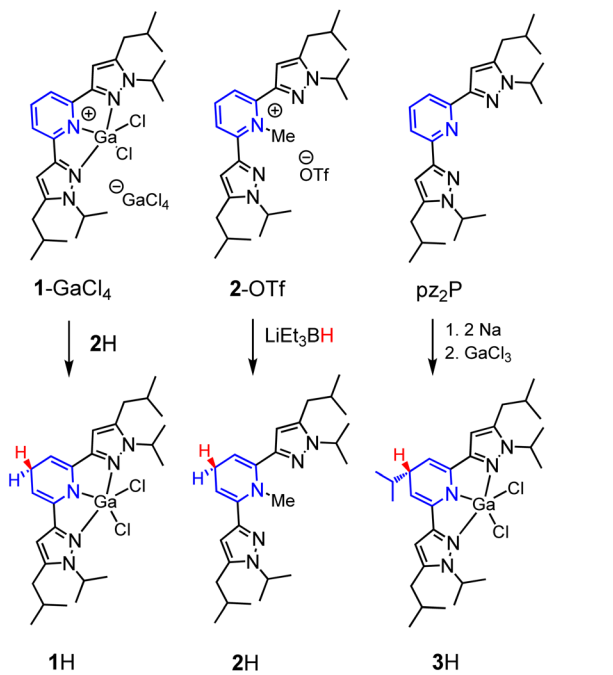

Scheme 3 Syntheses of **1H**, **2H** and **3H**.

Open Access Article. Published on 16 November 2023. Downloaded on 5/2/2026 7:54:51 PM.
This article is licensed under a Creative Commons Attribution 3.0 Unported Licence.

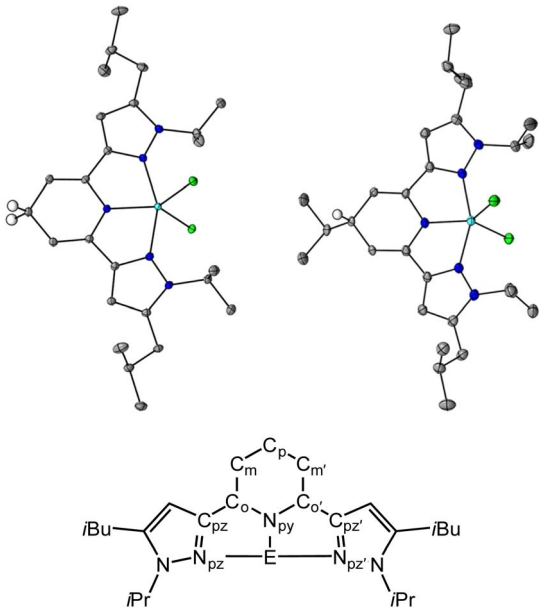

Fig. 1 Solid state structures of **1**H (top left) and **3**H (top right) and pz_2P atom naming convention used throughout (bottom). Blue, light blue, green, gray ellipsoids, and white circles represent N, Ga, Cl, C, and H atoms, respectively. H atoms except C_p–H omitted for clarity. The thermal ellipsoids are shown at 30% probability.

synthesis of **2**H is described in the next paragraph). The ^{1}H NMR spectrum of **1**H showed no aromatic resonances, but the C_p–H resonance is observed as a triplet at 3.48 ppm, and this is consistent with DHP^- formation as observed in **4**H, **2**H, and **3**H which have C_p–H resonances at 3.50, 3.62 and 3.57 ppm, respectively. The pyrazole ring proton resonance is a singlet, shifted upfield, from 7.01 in $\mathbf{1}^+$ to 5.92 ppm in **1**H (Fig. S2†). The composition of **1**H was further confirmed by X-ray diffraction and combustion analysis.

The synthesis of 1,4-DHP^-s from *N*-alkylated pyridinium salts has been reported, using sodium dithionate,[38] or a metal hydride donor as reductant.[39] For the preparation of **2**H we found that addition of 1.3 equivalents of lithium triethyl borohydride, $LiEt_3BH$, to a colourless solution of **2**-OTf in THF resulted in an instant colour change to a yellow solution. After stirring for 5 minutes the solution was concentrated to a residue which was dissolved in hexane and filtered. The yellow oily filtrate yielded $pz_2(N\text{-}Me^HP)$, **2**H, in 27% yield following workup. The proton NMR spectrum of **2**H is consistent with the 1,4-DHP^- structure and with NMR resonances at 5.62 and 3.24 ppm (Fig. S3†). The composition of **2**H was confirmed using HRMS.

Solid state structures

Crystals suitable for single crystal X-ray diffraction of the 1,4-DHP^- ligand compounds, **1**H and **3**H, were obtained from saturated solutions of MeCN and hexane respectively over a period of three days, and were obtained as purple, and colorless block shaped crystals, respectively (Tables S1 and S2,† Fig. 1). We were not able to obtain crystals of **2**H despite many attempts. For **1**H, the average bond lengths of the N_{py}–C_o, C_o–C_m and C_p–C_m bonds are 1.387(6), 1.343(7) and 1.507(7) Å, respectively, and for **3**H these are 1.433(6), 1.33(2) and 1.507(8) Å, respectively (see Fig. 1 for pz_2P atom naming). The increased bond lengths for C_p–C_m in both **1**H and **3**H relative to $\mathbf{1}^+$, are characteristic of 1,4-DHP^- structures. Upon formation of the 1,4-DHP^-, the geometry around the Ga(III) center becomes closer to trigonal bipyramidal with a τ_5 value of 0.76 for both **1**H and **3**H.[40] There is also an increase in the N_{pz}–Ga–$N_{pz'}$ bond angle from 154.9(1)° in $\mathbf{1}^+$ to 156.47(3)° and 156.51(8)° in **1**H and **3**H respectively.[30] The ligand twists to accommodate the distorted trigonal bipyramidal geometry as indicated by the torsion angle between the two coordinating pyrazine arms C_{pz}=$N_{pz}C_{pz'}$=$N_{pz'}$, which increase by 2.89° and 1.91° for **1**H and **3**H respectively relative to $\mathbf{1}^+$. There is no significant difference in the bond distances within the pyrazole rings between all compounds discussed (Tables S3 and S4†).

Hydride transfer reactions of 1H, 2H and 4H

There are several possible experiments that can be used to obtain ΔG_{H^-}.[22] We found hydride transfer best suited for **1**H, **2**H and **4**H where chemical equilibria were established between **1**H, **2**H and **4**H, and organohydride molecules of known ΔG_{H^-}. Using this method, direct HT from a donor (D–H) to acceptor (A^+) is observed and then an equilibrium constant can be determined which establishes the difference in ΔG_{H^-} between the donor and acceptor. The relationship between the hydride donor ability of D–H and A–H, and the hydride transfer between D^+ and A^+ is described by eqn (2)–(5):[22]

$$\text{D–H} + \text{A}^+ \rightleftharpoons \text{D}^+ + \text{A–H}\ K_{(2)} \quad (2)$$

$$\text{A–H} \rightleftharpoons \text{A}^+ + \text{H}^-\ \Delta G_{H^-}(\text{A–H}) \quad (3)$$

$$\text{D–H} \rightleftharpoons \text{D}^+ + \text{H}^-\ \Delta G_{H^-}(\text{D–H}) \quad (4)$$

where $\Delta G_{H-(4)} = \Delta G_{H-(2)} - \Delta G_{H-(3)}$

and

$$\Delta G_{H-(2)} = -RT\ln(K_{(2)}) \quad (5)$$

We first set out to determine the hydricity of **2**H, because **2**H is the easiest of the hydrides to make, with a series of hydride acceptors of known hydricity. Reaction of **2**-OTf with one equivalent of 1,3-dimethyl-2-phenyl-2,3-dihydro-1*H*-benzo[*d*]imidazole, BnHPh ($\Delta G_{H^-} = 50$ kcal mol^{-1} in MeCN, (Chart 1))[19] resulted in HT which was observed by ^{1}H NMR in CD_3CN after 2 days and approached equilibrium after two weeks, as in eqn (6):

$$\text{BnHPh} + \mathbf{2}^+ \rightleftharpoons \text{BnPh}^+ + \mathbf{2}\text{H} \quad (6)$$

$$\text{Bn}^+ + \mathbf{2}\text{H} \rightleftharpoons \text{BnH} + \mathbf{2}^+ \quad (7)$$

HT from **2**H to one equivalent of 1,3-dimethyl-1*H*-benzimidazolium, Bn^+ ($\Delta G_{H^-} = 45$ kcal mol^{-1} in MeCN (Chart 1))[29] was also observed by ^{1}H NMR after 3 days and approached equilibrium after two weeks (eqn (7), Fig. S4 and S5†). The equilibria were heavily reactant favoured suggesting that the hydricity of **2**H lies close to the middle of the range from 45–50 kcal mol^{-1}

© 2023 The Author(s). Published by the Royal Society of Chemistry

Open Access Article. Published on 16 November 2023. Downloaded on 5/2/2026 7:54:51 PM.
This article is licensed under a Creative Commons Attribution 3.0 Unported Licence.

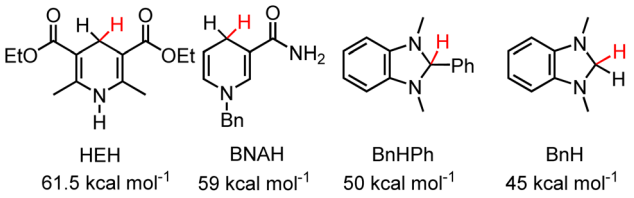

Chart 1 1,4-DHPs and benzimidazoles discussed in the text and their reported hydricities in MeCN.[21]

in MeCN solution. Control experiments run in parallel consisting of the starting materials **2**-OTf, **2**H, 1,3-dimethyl-2-phenyl-2,3-dihydro-1*H*-benzo[*d*]imidazole and 1,3-dimethyl-1*H*-benzimidazolium iodide in CD_3CN with trimethoxybenzene as an internal standard show no changes after 2 weeks (Fig. S6–S9†). We, therefore, estimate for **2**H that $\Delta G_{H^-} = 47.5 \pm 2.5$ kcal mol^{-1}. These measurements put the ΔG_{H^-} of **2**H on the lower side (stronger hydride donor) of values reported for 1,4-DHPs which have been reported from 73–43 kcal mol^{-1}.[21] As a reference point to commonly employed DHPs, the Hantsch ester (HEH) has $\Delta G_{H^-} = 61.5$ kcal mol^{-1} and BNAH (1-benzyl-1,4-dihydronicotinamide) has $\Delta G_{H^-} = 59$ kcal mol^{-1}. An established trend is that DHP$^-$s are more hydridic when they are functionalized with electron donating groups. Both the Hantzsch ester and BNAH feature electron withdrawing groups (Chart 1), whereas **2**H has two moderately electron donating pyrazole groups. The hydricity of **2**H is similar to methyl substituted *N*-alkylated DHP$^-$s.[21]

Having established the hydricity of **2**H, we endeavoured to determine if HT from **2**H would be observed to either **1**$^+$ or **4**$^+$. Reactions of a 1 : 1 molar ratio of **1**-$GaCl_4$ with **2**H, and of [(pz_2P)$AlCl_2$]$AlCl_4$, **4**-$AlCl_4$, with **2**H were monitored by ^{1}H NMR in C_6D_6 in order to determine the reaction equilibria (Scheme 4).[1,41] The back reaction in these equilibria corresponds to eqn (2) and were used in calculations of ΔG_{H^-}. Integration of ^{1}H NMR signals (C_p–*H* of **4**$^+$/**4**H and **1**$^+$/**1**H and N_{py}–CH_3 of **2**$^+$/**2**H) relative to the internal standard trimethoxybenzene showed equilibria were established after 4 days for reaction of **1**$^+$ and **2**H and after 3 days for the reaction of **4**$^+$ and **2**H (see ESI for full experimental details†). We recognize that solvents such as DMSO, MeCN or H_2O, which have higher dielectric constants and a wealth of reported hydricity data, would be a better choice for monitoring these equilibria,[23] but **1**-$GaCl_4$ is insoluble in DMSO, **1**H is sparingly soluble in MeCN, and both **4**$^+$ and **1**$^+$ are unstable in protic solvents. Equilibrium constants (K) were calculated as 0.83 for the back reaction of **1**-$GaCl_4$ with **2**H and 0.24 for the back reaction of **4**-$AlCl_4$ with **2**H. These values correspond to a difference in ΔG_{H^-} between **1**H and **2**H of 0.1 ± 0.1 kcal mol^{-1} and a difference in ΔG_{H^-} between **4**H and **2**H of 0.8 ± 0.1 kcal-mol^{-1}. Given that the values of **1**H, **2**H and **4**H were all found to be within 1 kcal mol^{-1} in benzene, which has a dielectric constant over 15 times lower than MeCN, we estimate that the hydricity values of **1**H and **4**H in MeCN would differ from **2**H by no more than 1 kcal mol^{-1}.[25,28,42] Minor differences in ΔG_{H^-} might arise from the varied Lewis acidity of the cations.

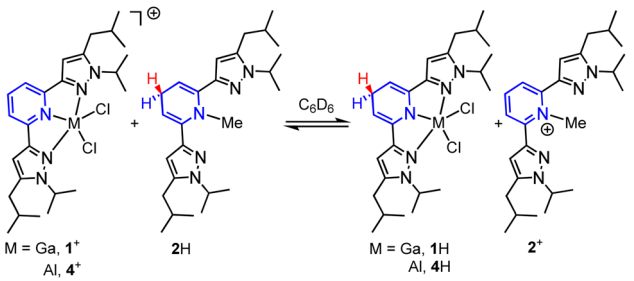

Scheme 4 HT equilibria between **1**-$GaCl_4$ and **2**H, and **4**-$AlCl_4$ and **2**H. Counter ions omitted for clarity.

Metal ion effects on the scaling relationship between E_p and ΔG_{H^-} for organohydrides

Linear correlations between hydricity (ΔG_{H^-}) of a transition metal hydride and the first reversible redox couple, $E_{1/2}(D^{+/0})$ in Scheme 1, of a parent transition metal complex are well established within several classes of metal complexes.[24,43,44] Concomitant reports by the groups of Kubiak,[20] and Glusac,[21] showed that a more general correlation exists across several classes of transition metal and ligand sets, and across structurally diverse organohydrides.

It is known that many oxidized organohydride precursors display irreversible reduction events, E_p, in CV experiments and we wondered if there is any correlation between a plot of E_p *vs.* ΔG_{H^-} for those compounds and whether the plot might highlight a variation in kinetic contributions to reduction that are causing the irreversibility. To construct a plot of E_p *vs.* ΔG_{H^-} we used reported, computationally obtained ΔG_{H^-} values for *N*-containing heterocyclic organohydrides in MeCN solution,[21] with their reported irreversible cathodic peak potentials (E_p) obtained using CV in MeCN solution.[33,36] We compiled E_p values for various imidazoles,[33] and substituted 1,4-DHPs;[36] and all E_p values were converted to V *vs.* SCE. Linear regression provides a linear relationship (Fig. 2). We notice that when fit independently, predicted E_p values for 1,4-DHPs are at more positive potentials than benzimidazoles with comparable ΔG_{H^-} within the reported ΔG_{H^-} range. Furthermore, another anodic shift in predicted E_p values is observed from fits of experimental ΔG_{H^-} values of 1,4-DHPs,[45–48] compared to those reported from computational methods. Experimentally measured values of ΔG_{H^-} (for **1**H and **2**H) and of E_p (for **1**$^+$ and **2**$^+$) were added to the plot of E_p *vs.* ΔG_{H^-} for comparison (red symbols, Fig. 2). Relative to the correlation line, **1**$^+$ is more easily reduced: E_p(**1**$^+$) is +215 mV more anodic than predicted. The Al-supported DHP compound **4**H has a similar E_p to **2**H when both are measured in THF, and this suggests that both $AlCl_2^+$ and $GaCl_2^+$ similarly break the E_p *vs.* ΔG_{H^-} scaling relationship, but there is not enough data available in THF to illustrate this point on a plot as we do for MeCN in Fig. 2. All the organohydrides plotted have cationic oxidized forms so the overall charge on the molecules should not be a factor contributing to E_p.

The combined data for **1**H, **2**H (and **1**$^+$, **2**$^+$) and the deviation of **1**$^+$ from the E_p *vs.* ΔG_{H^-} correlation lines are consistent with differences in reorganization energy that can be rationalized by

Open Access Article. Published on 16 November 2023. Downloaded on 5/2/2026 7:54:51 PM.
This article is licensed under a Creative Commons Attribution 3.0 Unported Licence.

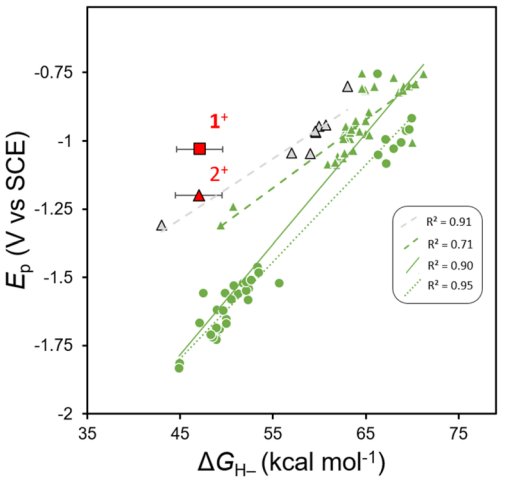

Fig. 2 Plot of E_p *vs.* ΔG_{H-} for benzimidazoles (circles), 1,4-DHPs (triangles) **2**$^+$ and those previously published and complexe **1**$^+$. Black outlines around markers represent experimentally determined ΔG_{H-} values, green markers indicate computational ΔG_{H-} values and red markers corresponds to compounds reported herein. The figure key displays R^2 values for linear fits to: 1,4-DHPs with experimentally determined ΔG_{H-} values (dashed grey line).[36,45–48] 1,4-DHPs with computationally determined ΔG_{H-} values (dashed green line),[21,36] 1,4-DHPs and benzimidazoles with computationally determined ΔG_{H-} values (solid green line),[21,33,36] and benzimidazoles with computationally determined ΔG_{H-} values (dotted green line).[21,33] **4**$^+$ is not included on the plot since it is not stable in MeCN.

the structural changes between the **1**$^+$ and **1**H pair. We expect no large structural changes upon conversion to **1**H and so it is reasonable to expect that kinetic contributions to E_p might be relatively low. In contrast, there are obvious structural differences between the **2**$^+$/**2**H pair. For **2**$^+$ we know that the flanking pyrazolyl rings of pz_2P have *N*-donor atoms oriented in toward the cationic *N*-Me-pyridyl group, and in **2**H those *N*-donor atoms of the pyrazolyl rings rotate away since the py ring is no longer cationic, as in the known structure of pz_2P where the pyrazolyl N atoms rotate out.[36] An additional effect of the Group 13 cation may be to stabilize the DHP$^-$ *via* bonding interactions between the N_{py} π-electrons and p_z orbital of the metal: electron donation from N_{py} to group 13 3+ cations have been observed in other complexes of tridentate pyridyl-centered ligands,[49] and may stabilize the DHP$^-$.[50]

Conclusion

New compounds **1**H and **2**H were prepared by a direct reaction of a hydride donor with the neutral ligand complexes **1**$^+$, and **2**$^+$, respectively: this hydride transfer reaction is a formal two-electron reduction and single protonation. Measurements of the E_p and ΔG_{H-} for **1**$^+$, **2**$^+$, and **4**$^+$, show that **1**$^+$ and **4**$^+$ do not follow the E_p *vs.* ΔG_{H-} scaling relationship. Both **1**$^+$ and **4**$^+$ have *N*-pyridyl coordination to Group 13 3+ cations, whereas **2**$^+$ is *N*-alkylated. These data were collected in THF and MeCN where possible, and the work in MeCN additionally permitted some quantification of this effect, where **2**$^+$ is shifted anodically from the E_p *vs.* ΔG_{H-} relationship by 215 mV (Fig. 2). Some of the observed anodic shift may arise from the cationic nature of $[(pz_2P)E]^+$ but it is unlikely that the full 215 mV anodic shift can be attributed to a single positive charge given that all of the model organohydrides on the plot have equivalent cationic charge. Based on these results, we propose that *N*-coordination of a Group 13 3+ cation to pyridyl offers a strategy for kinetic lowering of E_p. Future work on well-designed *N*-metallated DHP$^-$s will target electrochemically-driven HT reaction chemistry.

Author contributions

Leo Parsons collected and analyzed the data, and was involved in writing the manuscript. James Fettinger was involved in refinement of solid state structural X-ray data. Louise Berben was responsible for project design and management, and writing the manuscript.

Conflicts of interest

There are no conflicts to declare.

Acknowledgements

This manuscript is based on work supported by the National Science Foundation with award CHE-2054529.

Notes and references

1 R. B. Weerasooriya, J. L. Gesiorski, A. Alherz, S. Ilic, G. N. Hargenrader, C. B. Musgrave and K. D. Glusac, Kinetics of Hydride Transfer from Catalytic Metal-Free Hydride Donors to CO_2, *J. Phys. Chem. Lett.*, 2021, **12**, 2306–2311.
2 D. Ghosh, K. Kobayashi, T. Kajiwara, S. Kitagawa and K. Tanaka, Catalytic Hydride Transfer to CO_2 Using Ru-NAD-Type Complexes under Electrochemical Conditions, *Inorg. Chem.*, 2017, **56**, 11066–11073.
3 C. Zheng and S.-L. You, Transfer Hydrogenation with Hantzsch Esters and Related Organic Hydride Donors, *Chem. Soc. Rev.*, 2012, **41**, 2498–2518.
4 Q.-X. Xie, L.-X. Liu, Z.-H. Zhu, C. Yu and Y.-G. Zhou, Asymmetric Transfer Hydrogenation of 2,3-Disubstituted Flavanones through Dynamic Kinetic Resolution Enabled by RetroOxa-Michael Addition: Construction of Three Contiguous Stereogenic Centers, *J. Org. Chem.*, 2022, **87**, 7521–7530.
5 B. Gao, W. Meng, X. Feng and H. Du, Regenerable Dihydrophenanthridine via Borane-Catalyzed Hydrogenation for the Asymmetric Transfer Hydrogenation of Benzoxazinones, *Org. Lett.*, 2022, **24**, 3955–3959.
6 F. Hollmann, D. J. Opperman and C. E. Paul, Biocatalytic Reduction Reactions from a Chemist's Perspective, *Angew. Chem., Int. Ed.*, 2021, **60**, 5644–5665.
7 B. Desguin, J. Urdiain-Arraiza, M. Da Costa, M. Fellner, J. Hu, R. P. Hausinger, T. Desmet, P. Hols and P. Soumillion,

© 2023 The Author(s). Published by the Royal Society of Chemistry

Open Access Article. Published on 16 November 2023. Downloaded on 5/2/2026 7:54:51 PM. This article is licensed under a Creative Commons Attribution 3.0 Unported Licence.

Uncovering a superfamily of nickel-dependent hydroxyacid racemases and epimerases, *Sci. Rep.*, 2020, **10**, 18123.

8 F. G. Mutti, T. Knaus, N. S. Scruttion, M. Breuer and N. J. Turner, Conversion of Alcohols to Enantiopure Amines Through Dual-Enzyme Hydrogen-Borrowing Cascades, *Science*, 2015, **349**, 1525–1529.

9 S. L. Montgomer, J. Magnas-Sanchez, M. P. Thompson, G. A. Aleku, B. Dominguez and N. J. Turner, Direct Alkylation of Amines with Primary and Secondary Alcohols through Biocatalytic Hydrogen Borrowing, *Angew. Chem., Int. Ed.*, 2017, **56**, 10491–10494.

10 S. G. Ouellet, J. B. Tuttle and D. W. C. MacMillan, Enantioselective Organocatalytic Hydride Reduction, *J. Am. Chem. Soc.*, 2005, **127**, 32–33.

11 A. M. F. Phillips and A. J. L. Pomberio, Recent Advances in Organocatalytic Enantioselectrive Transfer Hydrogenation, *Org. Biomol. Chem.*, 2017, **15**, 2307–2340.

12 Z.-H. Zhu, Y.-X. Ding and Y.-G. Zhou, Transfer-Catalyst-Free Biomimetic Asymmetric Reduction of 3-Sulfonyl Coumarins with a Regenerable NAD(P)H Model, *Chem. Commun.*, 2022, **58**, 3973–3976.

13 Y. Gu, J. R. Norton, F. Salahi, V. G. Lisnyak, Z. Zhou and S. A. Snyder, Highly Selective Hydrogenation of C-C Bonds Catalyzed by a Rhodium Hydride, *J. Am. Chem. Soc.*, 2021, **143**, 9657–9663.

14 J. Wang, Z.-H. Zhu, M.-W. Chen, Q.-A. Chen and Y.-G. Zhou, Catalytic Biomimetic Asymmetric Reduction of Alkenes and Imines Enabled by Chiral and Regenerable NAD(P)H Models, *Angew. Chem., Int. Ed.*, 2019, **58**, 1813–1817.

15 A. B. Shabade, D. M. Sharma, P. Bajpai, R. G. Gonnade, K. Vanka and B. Punji, Room Temperature Chemoselective Hydrogenation Of C=C, C=O and C=N Bonds by Using a Well-defined Mixed Donor Mn(I) Pincer Catalyst, *Chem. Sci.*, 2022, **13**, 13764–13773.

16 A. Marrone and R. H. Fish, Bioorganometallic Chemistry at the Interface with Biocatalysis: Chemoselective Reduction of Biomimetic NAD^+ Cofactors with $[Cp^*Rh(bpy)H]^+$, Tandem Catalysis with 1,4-NADH-Dependent Enzymes, Chiral Synthesis, Organotin Metabolites, and DFT Mechanism Studies, *Organometallics*, 2023, **42**, 288–306.

17 P. Karak, S. Kumar, K. Mandal and J. Choudhury, Bis-Imidazolium-Embedded Heterohelicene: A Regenerable $NADP^+$ Cofactor Analogue for Electrocatalytic CO_2 Reduction, *J. Am. Chem. Soc.*, 2023, **145**, 7230–7241.

18 S. Ilic, A. Alherz, C. B. Musgrave and K. D. Glusac, Importance of Proton-Coupled Electron Transfer in Cathodic Regeneration of Organic Hydrides, *Chem. Commun.*, 2019, **55**, 5583–5586.

19 S. Ilic, U. P. Kadel, Y. Basdogan, J. A. Keith and K. D. Glusac, Thermodynamic Hydricities of Biomimetic Organic Hydride Donors, *J. Am. Chem. Soc.*, 2018, **140**, 4569–4579.

20 K. M. Waldie, A. L. Ostericher, M. H. Reineke, A. F. Sasayama and C. P. Kubiak, Hydricity of Tansition-Metal Hydrides: Thermodynamic Considerations for CO_2 Reduction, *ACS Catal.*, 2018, **8**, 1313–1324.

21 S. Ilic, A. Alherz, C. B. Musgrave and K. D. Glusac, Thermodynamic and Kinetic Hydricities of Metal-Free Hydrides, *Chem. Soc. Rev.*, 2018, **47**, 2809–2836.

22 E. S. Wiedner, M. B. Chambers, C. L. Pitman, M. R. Bullock, A. J. M. Miller and A. M. Appel, Thermodynamic hydricity of transition metal hydrides, *Chem. Rev.*, 2016, **116**, 8655–8692.

23 K. R. Brereton, N. E. Smith, N. Hazari and A. Miller, Thermodynamic and kinetic hydricity of transition metal hydrides, *Chem. Soc. Rev.*, 2020, **49**, 7929–7984.

24 N. D. Loewen, T. V. Neelakantan and L. A. Berben, Renewable Formate from C−H Bond Formation with CO2: Using Iron Carbonyl Clusters as Electrocatalysts, *Acc. Chem. Res.*, 2017, **50**, 2362–2370.

25 A. Taheri and L. A. Berben, Tailoring Electrocatalysts for Selective CO2 or H+ Reduction: Iron Carbonyl Clusters as a Case Study, *Inorg. Chem.*, 2016, **55**, 378–385.

26 B. M. Caballos and J. Y. Yang, Directing the Reactivity of Metal Hydrides for Selective CO_2 Reduction, *Proc. Natl. Acad. Sci. U. S. A.*, 2018, **115**, 12686–12691.

27 J. M. Barlow and J. Y. Yang, Thermodynamic Considerations for Optimizing Selective CO_2 Reduction by Molecular Catalysts, *ACS Cent. Sci.*, 2019, **5**, 580–588.

28 Y. Matsubara, E. Fujita, M. D. Doherty, J. T. Muckerman and C. Creutz, Thermodynamic and Kinetic Hydricity of Ruthenium(II) Hydride Complexes, *J. Am. Chem. Soc.*, 2012, **134**, 15743–15757.

29 W. W. Ellis, J. W. Raebiger, C. J. Curtis, J. W. Bruno and D. L. DuBois, Hydricities of BzNADH, $C_5H_5Mo(PMe_3)(CO)_2H$, and $C_5Me_5Mo(PMe_3)(CO)_2H$ in Acetonitrile, *J. Am. Chem. Soc.*, 2004, **126**, 2738–2743.

30 L. W. T. Parsons, J. C. Fettinger and L. A. Berben, Group 13 ion coordination to pyridyl models NAD+ reduction potentials, *Chem. Commun.*, 2023, **59**, 9110–9113.

31 E. J. Thompson and L. A. Berben, Electrocatalytic Hydrogen Production by an Aluminum(III) Complex: Ligand-Based Proton and Electron Transfer, *Angew. Chem., Int. Ed.*, 2015, **54**, 11642–11646.

32 K. T. Horak, D. G. VanderVelde and T. Agapie, Tuning of Metal Complex Electronics and Reactivity by Remote Lewis Acid Binding to π-Coordinated Pyridine Diphosphine Ligands, *Organometallics*, 2015, **34**, 4753–4765.

33 X.-Q. Zhu, M.-T. Zhang, A. Yu, C.-H. Wang and J. P. Cheng, Hydride, Hydrogen Atom, Proton, and Electron Transfer Driving Forces of Various Five-Membered Heterocyclic Organic Hydrides and Their Reaction Intermediates in Acetonitrile, *J. Am. Chem. Soc.*, 2008, **130**, 2501–2516.

34 X.-Q. Zhu, Y. Tan and C.-T. Cao, Thermodynamic Diagnosis of the Properties and Mechanism of Dihydropyridine-Type Compounds as Hydride Source in Acetonitrile with "Molecule ID Card", *J. Phys. Chem. B*, 2010, **114**, 2058–2075.

35 T. W. Myers and L. A. Berben, A sterically demanding iminopyridine ligand affords redox-active complexes of aluminum(III) and gallium(III), *Inorg. Chem.*, 2012, **51**, 1480–1488.

36 T. J. Sherbow, J. C. Fettinger and L. A. Berben, Control of Ligand pKa Values Tunes the Electrocatalytic Dihydrogen

Open Access Article. Published on 16 November 2023. Downloaded on 5/2/2026 7:54:51 PM.
This article is licensed under a Creative Commons Attribution 3.0 Unported Licence.

Evolution Mechanism in a Redox-Active Aluminum(III) Complex, *Inorg. Chem.*, 2017, **56**, 8651–8660.

37 G. Zhang, J. Wu, S. Zheng, M. C. Neary, J. Mao, M. Flores, R. J. Trovitch and P. A. Dub, Redox-noninnocent ligand-supported vanadium catalysts for the chemoselective reduction of C=X (X = O, N) functionalities, *J. Am. Chem. Soc.*, 2019, **141**, 15230–15239.

38 D. Mauzerall and F. H. Westheimer, 1-Benzyldihydronicotinamide – a model for reduced DPN, *J. Am. Chem. Soc.*, 1955, **77**, 2261–2264.

39 J. Zhang, J.-D. Yang and J.-P. Cheng, A Nucleophilicity scale for the reactivity of diazaphospholenium hydrides: structural insights and synthetic applications, *Angew. Chem., Int. Ed.*, 2019, **58**, 5983–5987.

40 A. W. Addison, T. N. Rao, J. Reedijk, J. van Rijin and G. C. Verschoor, Synthesis, Structure, and spectroscopic properties of copper(II) compounds containing nitrogen-sulphur donor ligands; the crystal and molecular structure of aqua[1,7-bis(N-methylbenzimidazol-2'-yl)-2,6-dithiaheptane]copper(II) perchlorate, *J. Chem. Soc., Dalton Trans.*, 1984, **7**, 1349–1356.

41 A. Kobayashi, H. Konno, K. Sakamoto, A. Sekine, Y. Ohashi, M. Iida and O. Isitani, Transition metal complexes coordinated by an NAD(P)H model compound and their enhanced hydride-donating abilities in the presence of a base, *Chem. Eur. J.*, 2005, **11**, 4219–4226.

42 C. Creutz and M. H. Chou, Rapid transfer of hydride ion from a ruthenium complex to C1 species in water, *J. Am. Chem. Soc.*, 2007, **129**, 10108–10109.

43 D. E. Berning, B. C. Noll and D. L. DuBois, Relative Hydride, Proton, and Hydrogen Atom Transfer Abilities of $[HM(diphosphine)_2]PF_6$ Complexes (M = Pt, Ni), *J. Am. Chem. Soc.*, 1999, **121**, 11432–11447.

44 N. Sarker and J. W. Bruno, Thermodynamic and Kinetic Studies of Hydride Transfer for a Series of Molybdenum and Tungsten Hydrides, *J. Am. Chem. Soc.*, 1999, **121**, 2174–2180.

45 Y. Matsubara, F. Etsuko, M. D. Doherty, J. T. Muckerman and C. Creutz, *J. Am. Chem. Soc.*, 2012, **134**, 15743–15757.

46 S. Ilic, U. P. Kadel, Y. Basdogan, J. A. Keith and K. D. Glusac, *J. Am. Chem. Soc.*, 2018, **140**, 4569–4579.

47 W. W. Ellis, J. W. Raebiger, C. J. Curtis, J. W. Bruno and D. L. DuBois, *J. Am. Chem. Soc.*, 2004, **126**, 2738–2743.

48 T.-Y. Cheng, B. S. Brunschwig and R. M. Bullock, *J. Am. Chem. Soc.*, 1998, **120**, 13121–13137.

49 T. M. Bass, C. R. Carr, T. J. Sherbow, J. C. Fettinger and L. A. Berben, Syntheses of Square Planar Gallium Complexes and a Proton NMR Correlation Probing Metalloaromaticity, *Inorg. Chem.*, 2020, **59**, 13517–13523.

50 E. Radcliffe, J. J. Dunsford, J. Cid, V. Fasano and M. J. Ingleson, N-Heterocycle-Ligated Borocations as Highly Tunable Carbon Lewis Acids, *Organometallics*, 2017, **36**, 4952–4960.

© 2023 The Author(s). Published by the Royal Society of Chemistry